Received: 12 August 2023 | Revised: 9 November 2023 | Accepted: 11 November 2023

DOI: 10.1002/jcc.27267

RESEARCH ARTICLE

Journal of COMPUTATIONAL CHEMISTRY WILEY

Iron–histidine bonding in bishistidyl hemoproteins–A local vibrational mode study

Marek Freindorf | Juliana J. Antonio | Elfi Kraka

Chemistry Department, Southern Methodist University, Dallas, Texas, USA

Correspondence
Marek Freindorf, Chemistry Department, Southern Methodist University, 3215 Daniel Avenue, Dallas, TX 75275-0314, USA.
Email: mfreindorf@smu.edu

Abstract

We investigated the intrinsic strength of distal and proximal FeN bonds for both ferric and ferrous oxidation states of bishistidyl hemoproteins from bacteria, animals, human, and plants, including two cytoglobins, ten hemoglobins, two myoglobins, six neuroglobins, and six phytoglobins. As a qualified measure of bond strength, we used local vibrational force constants k^a(FeN) based on local mode theory developed in our group. All calculations were performed with a hybrid QM/MM ansatz. Starting geometries were taken from available x-ray structures. k^a(FeN) values were correlated with FeN bond lengths and covalent bond character. We also investigated the stiffness of the axial NFeN bond angle. Our results highlight that protein effects are sensitively reflected in k^a(FeN), allowing one to compare trends in diverse protein groups. Moreover, k^a(NFeN) is a perfect tool to monitor changes in the axial heme framework caused by different protein environments as well as different Fe oxidation states.

KEYWORDS
bishistidyl hemoproteins, intrinsic bond strength, local mode analysis, local mode force constants, QM/MM

1 | INTRODUCTION

The heme group is widely distributed and essential in biological systems, such as hemoproteins.[1,2] As such, the heme group plays an important role as an active site in biomolecules performing a variety of functions involving transport and storage of endogenous molecules[3–5] (such as O_2, CO, and NO), electron transfer,[6] and catalysis.[7] The heme group in hemoproteins with a globin fold is attached to the protein backbone via the side chain of a proximal histidine, while the distal side of the heme pocket can be accessible by endogenous and exogenous molecules, leading to penta- or hexa- coordination to the central Fe atom, which can be in two oxidation states such as ferrous Fe(II) or ferric Fe(III).

In the past two decades, a new form of hexacoordinate hemoproteins has been discovered, where the distal side of the heme group is coordinated to a native distal histidine, in this study labeled as bishistidyl hemoproteins. These bishistidyl hemoproteins have been characterized experimentally via spectroscopy methods,[8–12] kinetic studies,[13–20] and reduction studies.[21] Also, some theoretical studies, such as molecular dynamics[22] and conformational studies,[23] have been conducted to supplement experimental structural and kinetic properties. As mentioned previously, hemoproteins can be in two oxidation states, ferrous or ferric. For bishistidyl hemoproteins, the native distal histidine binds to form the hexacoordinate heme group which can exist in either ferrous or ferric states, with varying affinities depending on the class of hemoproteins and can exhibit reversible

bishistidyl coordination of the heme iron, while still having the ability to bind to exogenous or endogenous ligands.[15] Therefore, the biochemical activity of bishistidyl hemoproteins appears to depend on the cleavage of the distal FeN chemical bond leaving the distal site of the heme pocket available for the coordination of endogenous ligands, while the precise biochemical mechanism of this process is still unknown.[18] The parameters of the FeN chemical bond in a simple gas phase model of the active site in bishistidyl hemoproteins have already been investigated theoretically,[24] however, according to our knowledge, the FeN bond strength in these hemoproteins has not yet been investigated theoretically.

Inspired by this, we completed these studies through an investigation at the molecular level, utilizing QM/MM methodology, where starting geometries are taken from x-ray experimental structures of available bishistidyl hemoproteins. We divided the 26 proteins studied in this work into five groups based on the protein characterization provided by authors of the corresponding x-ray structures, which are listed in Table 1. The list includes two cytoglobins (labeled in this study as **CFI** and **CHU**), ten hemoglobins (**HDR**, **HFB**, **HFN**, **HGB**, **HHR**, **HHU**, **HHA**, **HSH**, **HSC**, and **HST**), two myoglobins (**MBR** and **MWH**), six neuroglobins (**NHM**, **NHU**, **NHS**, **NKU**, **NMS**, and **NWR**), and six phytoglobins (**PAR**, **PBE**, **PCR**, **PPA**, **PRC**, and **PTR**). This list also includes hemoproteins from a variety of species such as bacteria, animals, human, and plants (phytoglobins), whose scientific and common names are shown in Table 1, along with corresponding PDB entries. As a reference, we also included a gas phase model **Gas** as depicted in Figure 1A.

The objective of our comprehensive study was to provide an additional tool to shed light on these 26 different bishistidyl hemoproteins focusing on the intrinsic strength of FeN bonding, including (1) to assess the strength of the FeN distal and proximal bond; (2) to explore if the FeN bond strengths of these five groups show a correlation between each group; (3) to investigate how the strength of the distal and proximal FeN bonds relate to each other; (4) to compare the difference between the ferric and ferrous states with regards to the FeN bond strengths; and (5) to describe the stiffness of the NFeN axial bond angle; utilizing the local vibrational mode analysis developed in our group[25,26] complemented with Bader's quantum theory of atoms in molecules (QTAIM) analysis [27] and the natural bond orbital analysis.[28]

TABLE 1 Labels, protein type, PDB entry, scientific name, and common name of hemoproteins investigated in this study.

Label	Protein	PDB ID	Scientific name	Common name	References
CFI	Cytoglobin	6Q6P	*Dissostichus Mawsoni*	Antarctic Toothfish	29
CHU	Cytoglobin	2DC3	*Homo Sapiens*	Human	30
HDR	Hemoglobin	2BK9	*Drosophila Melanogaster*	Fruit Fly	11
HFB	Hemoglobin	1S5X	*Trematomus Bernacchii*	Emerald Rockcod	31
HFN	Hemoglobin	1LA6	*Trematomus Newnesi*	Dusky Rockcod	32
HGB	Hemoglobin	2W31	*Geobacter Sulfurreducens*	Bacterium	33
HHR	Hemoglobin	1NS6	*Equus Caballus*	Horse	34
HHU	Hemoglobin	6NQ5	*Homo Sapiens*	Human	35
HHA	Hemoglobin	1Z8U	*Homo Sapiens*	Human	36
HSH	Hemoglobin	3MKB	*Isurus Oxyrinchus*	Shark	37
HSC	Hemoglobin	4MAX	*Synechococcus*	Cyanobacterium	38
HST	Hemoglobin	1RTX	*Synechocystis*	Cyanobacterium	39
MBR	Myoglobin	1MNI	*Sus Scrofa*	Pig	40
MWH	Myoglobin	4PQB	*Physeter Catodon*	Sperm Whale	41
NHM	Neuroglobin	7VQG	*Homo Sapiens*	Human	42
NHU	Neuroglobin	1OJ6	*Homo Sapiens*	Human	43
NHS	Neuroglobin	4MPM	*Homo Sapiens*	Human	44
NKU	Neuroglobin	5ZIQ	*Ramazzottius Varieornatus*	Water Bear	45
NMS	Neuroglobin	1Q1F	*Mus Musculus*	House Mouse	46
NWR	Neuroglobin	4BJA	*Caenorhabditis Elegans*	Roundworm	47
PAR	Phytoglobin	3ZHW	*Arabidopsis Thaliana*	Thale Cress	48
PBE	Phytoglobin	7ZOS	*Beta Vulgaris*	Beet	49
PCR	Phytoglobin	2R50	*Zea Mays-Parviglumis*	Corn	50
PPA	Phytoglobin	3QQR	*Parasponia Andersonii*	Plant	51
PRC	Phytoglobin	1D8U	*Oryza Sativa*	Rice	52
PTR	Phytoglobin	3QQQ	*Trema Tomentosa*	Poison Peach	51

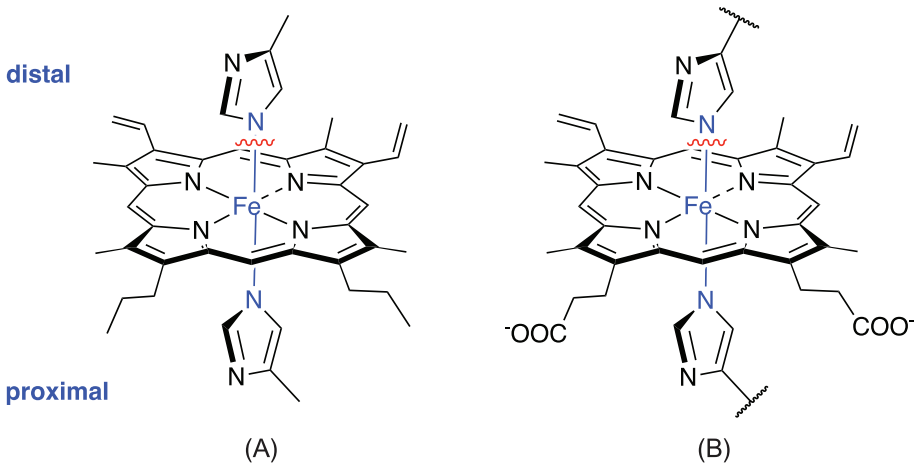

FIGURE 1 Schemes of bishistidyl iron complexes investigated in this study. (A) Gas phase model and (B) QM part of the hemoprotein active site.

1.1 | Bishistidyl hemoproteins studied

In the following, a short summary is given describing the bishistidyl hemoproteins members of each group investigated in this work.

Group 1, *cytoglobins*: includes the hemoprotein of the antarctic fish cytoglobin **CFI** from *Dissostichus Mawsoni*, and the human cytoglobin **CHU**. The x-ray dimeric structure of the fish cytoglobin **CFI** was reported with a resolution 3.0 Å, and was investigated in order to analyze its biological responses to low temperature.[29] The human cytoglobin **CHU**, whose x-ray dimeric structure was reported with a resolution of 1.68 Å, was investigated in order to analyze the extra N– and C–termini of the protein, and a new protein dimerization mode.[30]

Group 2, *hemoglobins*: includes 10 members. The drosophila hemoglobin **HDR** from *Drosophila Melanogaster*, whose x-ray monomeric structure was reported with a resolution of 1.2 Å, has been investigated in order to analyze the molecular mechanisms of the heme–ligand binding process.[11] The emerald rockcod hemoglobin **HFB** from *Trematomus Bernacchii* was reported with the x-ray tetrameric structure of a resolution of 2.4 Å, and has been the subject of a study analyzing its oxidation processes under extreme temperature conditions.[31] The x-ray tetrameric structure of the dusky rockcod hemoglobin **HFN** from *Trematomus Newnesi* was obtained with a resolution of 2.0 Å, and revealed that bishistidyl coordination has an intermediate structure between the relaxed and tense hemoglobin functional states.[32] The bacterium hemoglobin **HGB** from *Geobacter Sulfurreducens* was reported with the x-ray dimeric structure of a resolution of 1.5 Å and showed that in contrast to known six–coordinated globins, the distal histidine coordinated to Fe is located at a different topological site of the protein.[33] The x-ray tetrameric structure of the horse hemoglobin **HHR** from *Equus Caballus* has a resolution of 2.05 Å, and presents a pH–dependent transition from a water heme coordination to a bishistidine heme coordination.[34] The x-ray tetrameric structure of the human hemoglobin **HHU** with the bishistidyl coordination was reported with a resolution of 1.85 Å, showing both the alpha met coordination and the beta hemichrome coordination of the active site.[35] The x-ray dimeric structure of the other human hemoglobin **HHA** with the bishistidyl coordination was reported with a resolution of 2.4 Å and presents the structure of the oxidized α–hemoglobin bound to the α–hemoglobin–stabilizing protein, revealing a protective mechanism for the heme group.[36] The analysis of the shark hemoglobin **HSH** from *Isurus Oxyrinchus* was based on the x-ray tetrameric structure of a resolution of 1.9 Å, and showed an unliganded deoxy tense state conformation, which was a result of an association of several protein chains into a closely packed arrangement.[37] The cyanobacterium hemoglobin **HSC** from *Synechococcus* was analyzed based on the x-ray monomeric structure with a resolution of 1.44 Å and presented an unusual distortion of the heme group.[38] The x-ray monomeric structure of the other cyanobacterium hemoglobin **HST** from *Synechocystis* was reported with a resolution of 1.80 Å, and showed that side chains of important amino acids, which are located inside the heme pocket in similar hemoglobins, are forced out into the external solvent.[39]

Group 3, *myoglobins*: includes two members. The pig myoglobin **MBR** from *Sus Scrofa* was investigated based on the x-ray monomeric structure of a resolution of 2.07 Å, where the bishistidyl coordination was achieved by a protein double mutation H64V/V68H.[40] Similarly, the sperm whale myoglobin **MWH** from *Physeter Catodon* was analyzed based on the x-ray monomeric structure of a resolution of 1.94 Å, where the bishistidine coordination was obtained by a distal hydrogen–bonding network involving glutamic acid and another histidine.[41]

Group 4, *neuroglobins*: includes six members. The human neuroglobin **NHM** is the first member of this group, which was investigated based on the x-ray monomeric structure of a resolution 1.35 Å and involved disulfide bonds as an effect of the A15C protein mutation.[42] The wild type of the human neuroglobin is represented in our study by the x-ray monomeric structure of another human neuroglobin **NHU** with a resolution of 1.95 Å, showing a reversible bishistidyl heme coordination and an elongated protein matrix cavity.[43] The next human neuroglobin with disulfide bonds is represented in our study by the x-ray dimeric structure of human neuroglobin **NHS**, with a resolution of 1.74 Å, which showed that the cleavage of the disulfide bond stabilizes the bishistidyl coordination of the heme group and leads to a decrease of the oxygen affinity.[44] The water bear neuroglobin **NKU**

from *Ramazzottius Varieornatus* was investigated based on the x-ray monomeric structure of a resolution of 1.50 Å, and was classified as neuroglobin by a similar heme geometry to the human neuroglobin.[45] The x-ray monomeric structure of the mouse neuroglobin **NMS** from *Mus Musculus* has a resolution of 1.50 Å, and has been studied in order to analyze the movement of distal histidine out of the coordination center, making the way for exogenous ligand binding.[46] The last member of the neuroglobin group is represented by the x-ray dimeric structure of the roundworm neuroglobin **NWR** from *Caenorhabditis Elegans*, which was reported with a resolution of 1.65 Å, and showed redox signaling capabilities essential for reproduction.[47]

Group 5, *phytoglobins*: includes six members, which were observed in plants. The first member of this group is the x-ray monomeric structure of the thale cress phytoglobin **PAR** from *Arabidopsis Thaliana*-which was reported with a resolution of 2.22 Å and showed a tunnel connecting the distal pockets of both the monomers, suggesting cooperative ligand binding as well the role in NO scavenging.[48] The x-ray monomeric structure of the wild type beet phytoglobin **PBE** from *Beta Vulgaris* has a resolution of 1.90 Å, and showed that a conserved cysteine residue has the functional and structural role in enzymatic stability of this protein.[49] The next member of the phytoglobin group is represented by the x-ray dimeric structure of the corn phytoglobin **PCR** from *Zea Mays – Parviglumis*, having a resolution of 2.20 Å, and is a nonsymbiotic phytoglobin classified to a hemoglobin 1 class.[50] The plant phytoglobin **PPA** from *Parasponia Andersonii* was investigated using the x-ray monomeric structure of a resolution of 2.16 Å and is a non–legume suitable for symbiotic nitrogen fixation.[51] The next member of the phytoglobin group of our study is represented by the x-ray dimeric structure of the rice phytoglobin **PRC** from *Oryza Sativa* with a resolution of 2.35 Å, and showed high affinity to the molecular oxygen by a rapid displacement of distal histidine.[52] The last member of the phytoglobin group is represented by the X–ray dimeric structure of the poison peach phytoglobin **PTR** from *Trema Tomentosa*, having a resolution of 1.84 Å, and is very similar in the primary structure to the plant phytoglobin **PPA** from *Parasponia Andersonii* reported above, but has a different oxygen-binding affinity.[51]

2 | METHODOLOGY

As discussed above, the biochemical activity of bishistidyl hemoproteins depends on the cleavage of the FeN bond between iron and the distal histidine making space for an endogenous ligand (see Figure 1B). Therefore, in this work, we explored the intrinsic strength of the distal FeN bond in comparison with that of the proxial FeN bond. We applied as a qualified assessment tool local vibrational mode force constants k^a derived from local vibrational mode analysis (LMA) developed in our group.[26,25] LMA extracts specific information about the electronic structure and bonding of a molecule from normal vibrational modes, which are produced during a routine frequency calculation. Normal vibrational modes are generally delocalized over a molecule,[53–56] therefore associated normal mode frequencies and normal mode force constants cannot serve as a direct measure of bond strength. The delocalization is caused by two types of normal mode coupling, kinematic and electronic coupling. The electronic coupling, which is reflected by the off-diagonal elements of the force constant matrix expressed in Cartesian coordinates **x** or internal coordinates **q**, is effectively removed during the frequency calculation via the Wilson GF-formalism.[55] This involves transforming from Cartesian coordinates **x** to normal mode coordinates **Q** and related normal modes, resulting in a diagonal force constant matrix $\mathbf{K}^Q$. However, this procedure does not eliminate the kinematic (mass) coupling reflected by the Wilson **G** matrix (the so-called called "inverse kinetic energy" matrix), which has often been overlooked. Konkoli and Cremer solved this problem by solving mass-decoupled Euler-Lagrange equations in which the masses of all atoms of the molecule are set to zero except for those of the molecular fragment (such as bond, angle, or dihedral) undergoing the localized vibration of interest.[57,58] By doing so, they are able to account for the effect of kinetic (mass) coupling, and to derive for each molecular fragment being described by an internal coordinate $\mathbf{q}_n$ the associated local vibrational mode $\mathbf{a}_n$, the associated local mode frequency ω^a, and force constant k^a.[25,26,57,58] Local mode force constants k^a have proven to be a reliable tool to quantify the strength of covalent chemical bonds including metal-ligand bonds and weak chemical interactions such as halogen, chalcogen, pnicogen, tetrel, or hydrogen bonding as summarized in References 25,26 which also provides an in-depth description of the underlying theory of LMA. Recent work on iron-ligand bonding in carboxy myoglobins and carboxy neuroglobins can be found in References 59,60 and a new assessment of non-covalent π–interactions in mutated aquomet-myoglobin proteins in Reference 61.

For better comparison, k^a values can be transformed into relative bond strength orders (BSO) via a power relationship of the form $BSO = A * (k^a)^B$ according to the generalized Badger rule derived by Cremer, Kraka, and co–workers.[62,63] The parameters A and B are obtained from two reference molecules with known BSO and k^a values, with the request that for a zero k^a value the corresponding BSO value is zero too. In our study, we used as references the FeH and FeN diatomic molecules in their quartet electronic states. Calculated Mayer bond orders[64–66] of 0.8711 for the single FeH bond and of 1.9288 for FeN double bond, together with the corresponding k^a values of 1.967 mDyn/Å and 3.393 mDyn/Å (PBE0/6–31G(d,p) level of theory),[67,68] resulted in parameters A = 0.3247 and B = 1.4584, respectively.

Optimal geometries and vibrational frequencies of all hemoproteins investigated in this work were calculated with the ONIOM QM/MM method,[69] starting from experimental x-ray structures (A–chains) of the corresponding hemoproteins listed in Table 1. Hydrogen atoms were placed according to the standard AMBER[70] computational procedure, and the proteins were neutralized using corresponding counter–ions. The heme center was surrounded by a sphere of TIP3P[71] water molecules, with a radius of 16 Å. After initial minimization at the MM level of theory, the proteins were divided into QM and MM parts, where the QM part included the heme group with substituents and both the distal and proximal histidine (see Figure 1B),

while the MM part included the rest of the proteins. Chemical bonds between the histidine side chains and the protein backbones were cut and free valences were filled with hydrogen atoms. The QM/MM geometry optimizations and frequency calculations were performed with the scaled electronic embedding using the PBE0/6–31G(d,p)/AMBER level of theory.[67,68] The reference gas phase model (see Figure 1A) was calculated at the PBE0/6–31G(d,p) level of theory. The PBE0 functional is a well-fitted theoretical functional for transition metals complexes,[67,72,73,74] which was successfully used in our previous QM/MM calculations of hemoproteins.[59] This functional also reproduces very accurately the FeN bond length in the gas phase model (**Gas**). Using the PBE0/6–31G(d,p) level of theory, the calculated FeN bond length (1.965 Å) of **Gas** in the ferric state is very close to the x–ray experimental value of this bond length in bis(1-methylimidazole) (meso-tetramesitylporphinato) Fe(III) (1.970 Å).[75] The calculations for each protein and **Gas** were performed for two protein states, the ferric Fe_{III} and the ferrous Fe_{II}, representing the oxidized and the reduced protein form, respectively. This led to four FeN bonds investigated for each protein, namely $Fe_{III}N_{dist}$, $Fe_{III}N_{prox}$, $Fe_{II}N_{dist}$, and $Fe_{II}N_{prox}$, where *dist* and *prox* indicate the distal and proximal histidine, respectively. Images of the active site of all investigated proteins in their optimized geometries are shown in the Supplementary Material (Figures S5–S13). Ferrous and ferric complexes were calculated with restricted (RDFT) and unrestricted (UDFT) methods.[76]

Geometry optimizations and frequency calculations were performed with Gaussian16.[77] The frequency calculations of all protein complexes and the gas phase model were completed without imaginary normal mode frequencies, indicating minima on the potential energy surfaces. The frequency calculations were followed by the local mode analysis of the FeN bonds using the LModeA program[78] and complemented with the QTAIM analysis using the AIMALL program[79] and the NBO analysis performed with the NBO package.[80]

3 | RESULTS AND DISCUSSION

In this section, FeN bond properties are analyzed including local mode force constants k^a(FeN) and associated bond strength order BSOs, FeN bond distances R(FeN) and energy densities H_ρ(FeN) taken at a bond critical point $\rho(\mathbf{r}_b)$, for both distal and proximal FeN bonds in

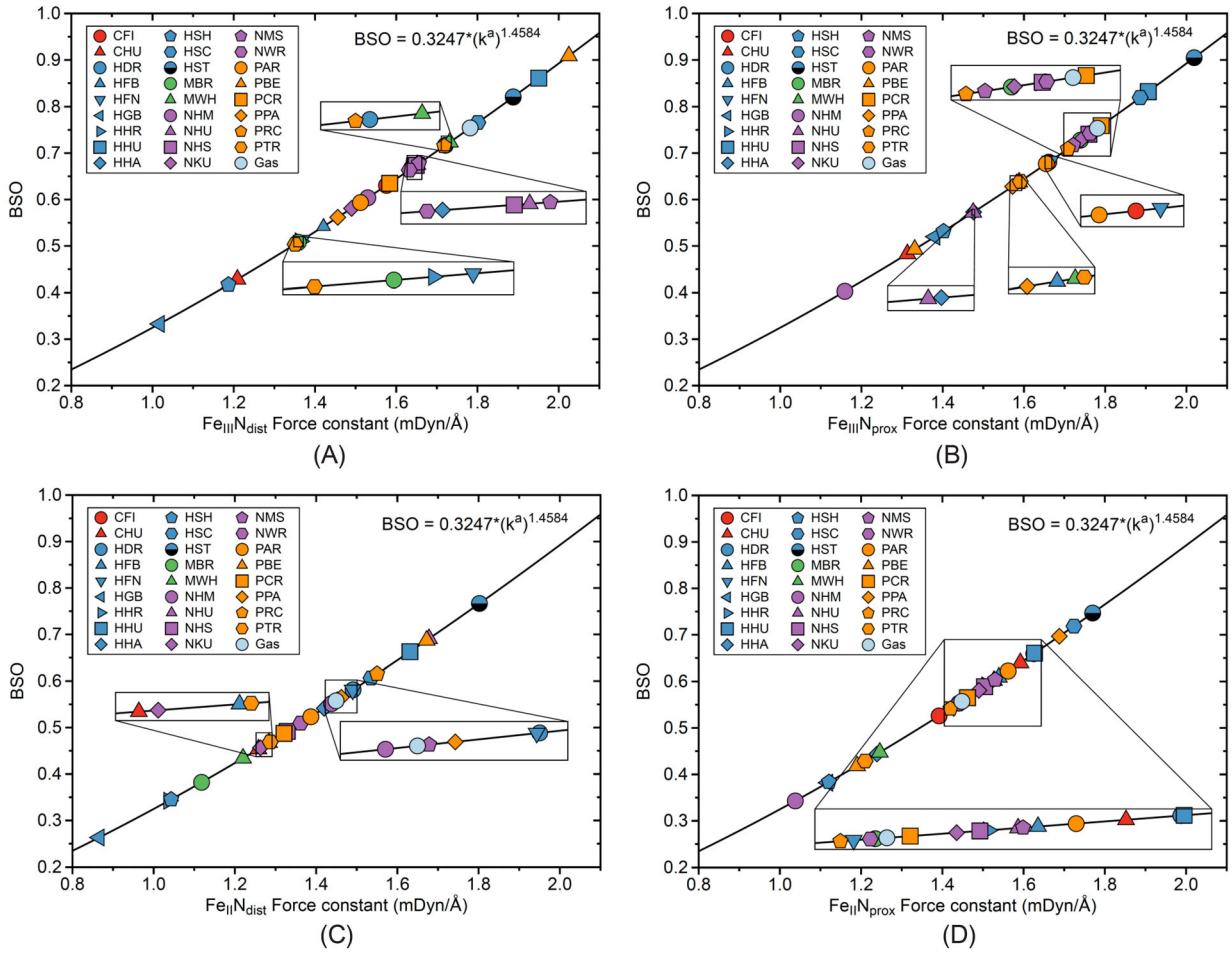

FIGURE 2 BSO as a function of k^a(FeN); (A) $Fe_{III}N_{dist}$; (B) $Fe_{III}N_{prox}$; (C) $Fe_{II}N_{dist}$; and (D) $Fe_{II}N_{prox}$ (for explanation see text). In order to differentiate between the five groups cytoglobins are given in red, hemoglobins in blue, myoglobins in green, neuroglobins in purple and phytoglobins in orange color. The heme gas phase model is given in light–blue color. For protein labels see Table 1.

their ferric and ferrous state, labelled in the following $Fe_{III}N_{dist}$ and $Fe_{III}N_{prox}$, $Fe_{II}N_{dist}$ and $Fe_{II}N_{prox}$, respectively. In addition, local force constants k^a(FeN) for the four different FeN scenarios are compared, as well as the atomic NBO charge difference Δ between Fe and N for distal and proximal FeN bonds. Finally, the relationship between k^a ($N_{prox}FeN_{dist}$), reflecting the stiffness of the $N_{prox}FeN_{dist}$ bond angles and k^a(FeN) force constants are investigated. Results are illustrated in Figures 2–8. The corresponding data can be found in Table S1 ($Fe_{III}N_{dist}$), Table S2 ($Fe_{III}N_{prox}$), Table S3 ($Fe_{II}N_{dist}$), Table S4 ($Fe_{II}N_{prox}$), and Table S5 ($N_{prox}Fe_{III}N_{dist}$ and N_{prox} $Fe_{II}N_{dist}$) of the Supplementary Material.

3.1 | Local FeN force constants and bond strengths

The first important result revealed by Figure 2A–D and the data in Tables S1–S4 is that there is no clustering of BSO values according to groups, which one may have expected. Even the strength of the FeN gas phase bond is found in the midst of the protein complex FeN bonds. This is a strong indication that the strength of the FeN bond to be cleaved in order to make room for another ligand, determining the diverse biological activity, is only one of the factors that play a role. BSO values cover the range of 0.2–0.95, that is, from very weak FeN bonds to bonds in the single bond range. The overall strongest FeN bond turned out to be the $Fe_{III}N_{dist}$ bond (Figure 2A, orange triangle) for beet phytoglobin **PBE** (k^a = 2.025 mDyn/Å, BSO = 0.909) of the phytoglobin group. On the other end of the spectrum, the overall weakest FeN bond we identified was the $Fe_{II}N_{dist}$ bond of the bacterium hemoglobin **HGB** (Figure 2C, blue triangle) (k^a = 0.866 mDyn/Å, BSO = 0.263). It is interesting to note the strength of the FeN gas phase bonds **Gas** (light–blue circle) adapt medium values ranging from k^a = 1.782 mDyn/Å, and BSO = 0.754 for $Fe_{III}N_{dist}$, to k^a = 1.449 mDyn/Å and BSO=0.558 for $Fe_{II}N_{dist}$, that is, they are weaker than the human hemoglobin **HHU**, cyanobacteria **HST**, or **HSC** FeN bonds, indicating the effect of the protein matrix on the FeN bond strength in hemoproteins.

As reflected in Figure 2A the $Fe_{III}N_{dist}$ bond strength of the fish cytoglobin **CFI** (red circle) from *Dissostichus Mawsoni* is located in the middle of our scale (k^a = 1.576 mDyn/Å, BSO = 0.630), while the human cytoglobin **CHU** $Fe_{III}N_{dist}$ bond (red triangle) is considerably weaker (k^a = 1.209 mDyn/Å). Both investigated myoglobins have

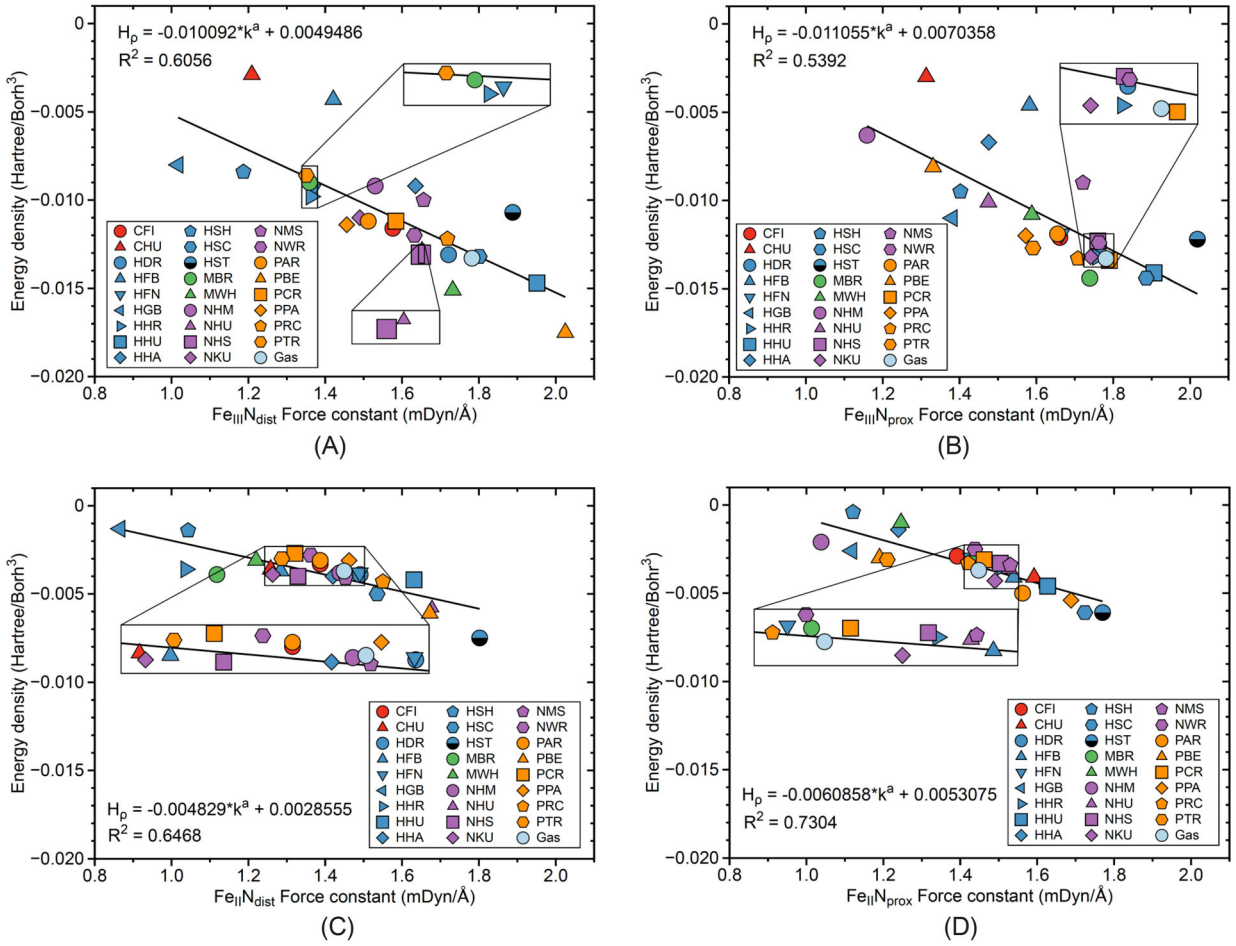

FIGURE 3 Correlation between H_p(FeN) and k^a(FeN); (A) $Fe_{III}N_{dist}$; (B) $Fe_{III}N_{prox}$; (C) $Fe_{II}N_{dist}$; and (**d**) $Fe_{II}N_{prox}$ (for explanation see text). In order to differentiate between the five groups cytoglobins are given in red, hemoglobins in blue, myoglobins in green, neuroglobins in purple and phytoglobins in orange color. The heme gas phase model is given in light–blue color. For protein labels see Table 1.

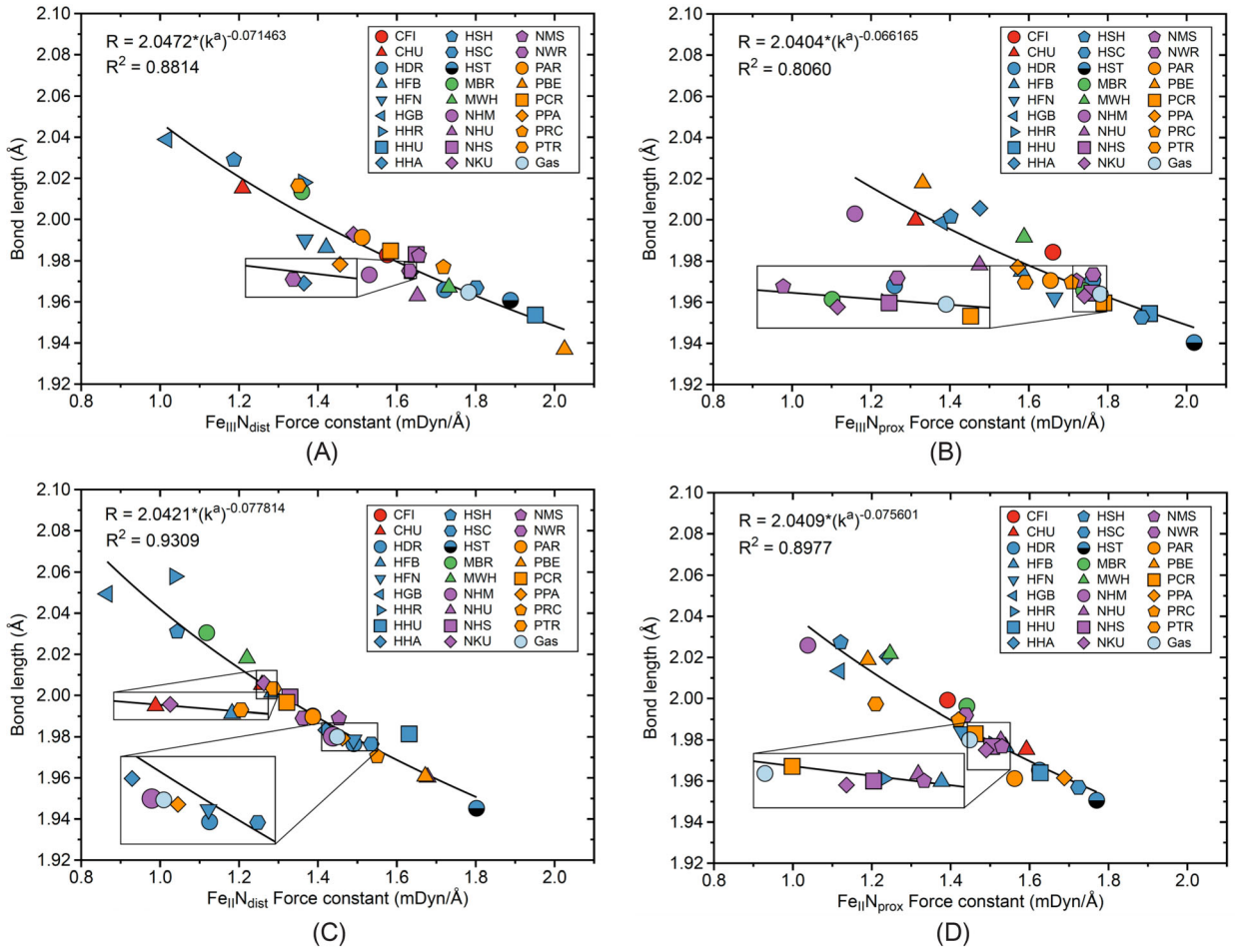

FIGURE 4 Correlation between R(FeN) and k^a(FeN); (A) $Fe_{III}N_{dist}$; (B) $Fe_{III}N_{prox}$; (C) $Fe_{II}N_{dist}$; and (D) $Fe_{II}N_{prox}$ (for explanation see text). In order to differentiate between the five groups cytoglobins are given in red, hemoglobins in blue, myoglobins in green, neuroglobins in purple and phytoglobins in orange color. The heme gas phase model is given in light–blue color. For protein labels see Table 1.

medium strong FeN bonds, with a stronger bond for whale myoglobin **MWH** (green triangle), and somewhat weaker FeN bond for pig myoglobin **MBR** (green circle). Similarly, the FeN bonds in the neuroglobin series (purple color) are of medium strength. Compared to the distal bonds, the proximal bonds are on average stronger, which holds in particular for the weaker FeN bonds (see Figure 2B). This is perfectly in line with the fact that the distal FeN bond needs to be broken to allow for biological activity to occur, such as small ligand binding. The same trend is mirrored by the $Fe_{II}N_{dist}$ and $Fe_{II}N_{prox}$ bond as shown in Figure 2C,D. It is interesting to note that compared to the ferric FeN bonds, the ferrous FeN are on average somewhat weaker, findings which could be useful for future experimental studies aiming at exploring differences in the biological activities of bishistidyl hemoproteins with iron in these two different oxidation states.

3.2 | Covalency of the FeN bonds

Figure 3A–D illustrate the correlation between the energy density at a bond critical point H_ρ(FeN) and the local mode force constant k^a(FeN). According to the Cremer-Kraka criterion, all FeN bonds investigated in this work are of slightly covalent character with some on the borderline of electrostatic interaction, with average H_ρ values ranging from −0.0035 to −0.0111 Hartree/Bohr^3. Similar to our previous studies on carboxy-myoglobins[59] and carboxy-neuroglobins,[60] we see the tendency that stronger iron-ligand bonds are characterized by larger covalency (i.e., a more negative H_ρ value). However, a caveat is appropriate. One has to keep in mind that H_ρ is taken at just one point, namely the bond critical point between the two atoms forming the bond, whereas the local stretching force constant as a second-order property of the potential energy surface involves the entire chemical bond.[25,26] Therefore, a significant correlation between these two properties can only be excepted when comparing more closely related molecular systems, such as carboxy-myoglobin[59] and carboxy-neuroglobins.[60]

As depicted in Figure 3A, we find the most covalent $Fe_{III}N_{dist}$ bond for beet phytoglobin **PBE** (orange triangle), with an H_ρ value of −0.0175 Hartree/Bohr^3, which is also the strongest $Fe_{III}N_{dist}$ bond. The least covalent bond in this series with an H_ρ value of −0.0029 Hartree/Bohr^3 (i.e., on the borderline of electrostatic interaction)

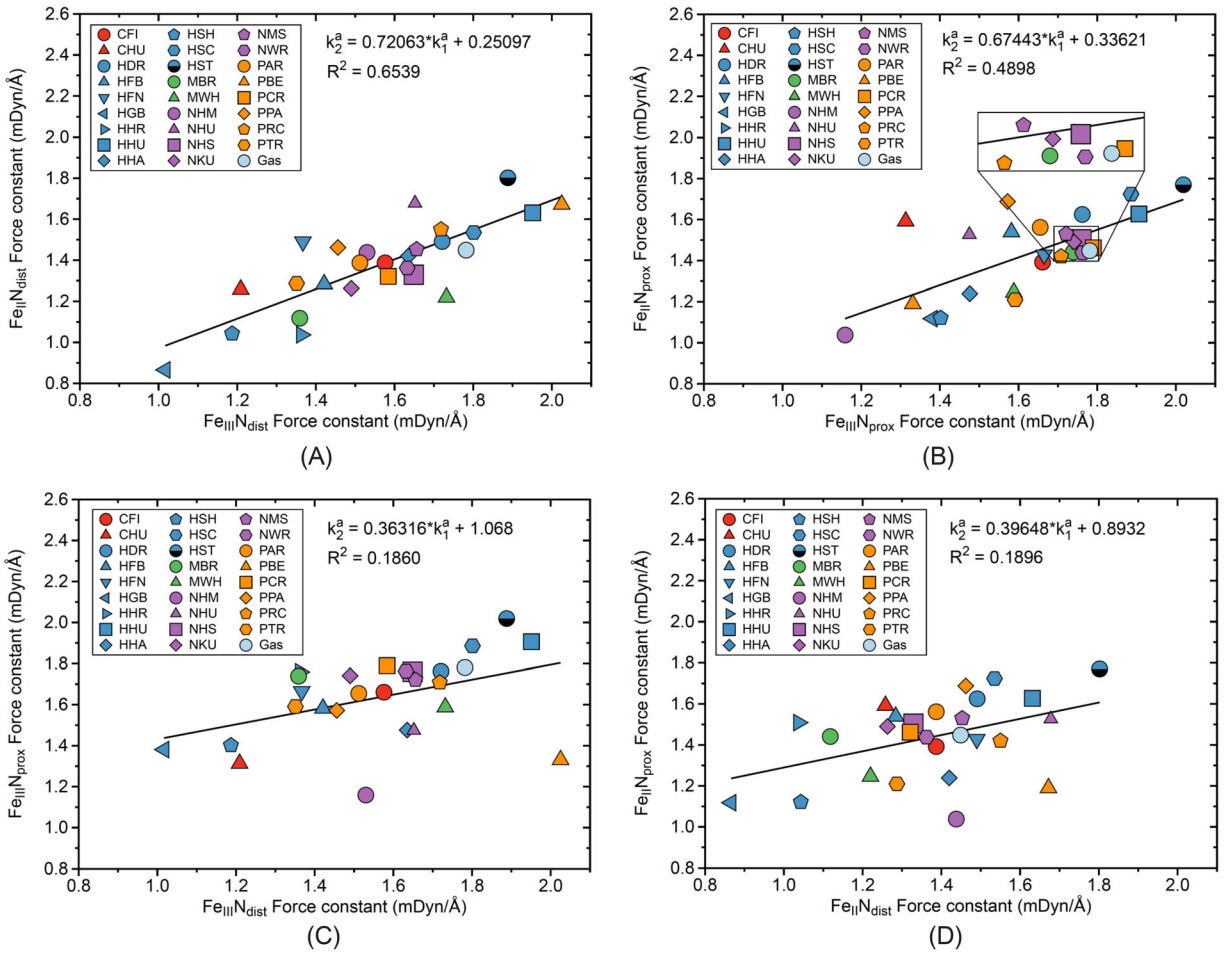

FIGURE 5 Correlation between different k^a(FeN); (A) $Fe_{III}N_{dist}$ versus $Fe_{II}N_{dist}$; (B) $Fe_{III}N_{prox}$ versus $Fe_{II}N_{prox}$; (C) $Fe_{III}N_{dist}$ versus $Fe_{III}N_{prox}$; and (D) $Fe_{II}N_{dist}$ versus $Fe_{II}N_{prox}$. In order to differentiate between the five groups cytoglobins are given in red, hemoglobins in blue, myoglobins in green, neuroglobins in purple and phytoglobins in orange color. The heme gas phase model is given in light–blue color. For protein labels see Table 1.

occurs for human cytoglobin **CHU** (red triangle), followed by the emerald rockcod hemoglobin **HFB** (upright blue triangle) with an H_ρ value of −0.0043 Hartree/Bohr^3, whereas the strength of both bonds is in the medium range. H_ρ values for the $Fe_{III}N_{prox}$ bond (see Figure 3B) show a similar relationship with the corresponding local force constants $k^a(Fe_{III}N_{prox})$. Again, the least covalent bonds are found for human cytoglobin **CHU** (red triangle) with an H_ρ value of −0.0030 Hartree/Bohr^3, followed by the emerald rockcod hemoglobin **HFB** (upright blue triangle) with an H_ρ value of −0.0046 Hartree/Bohr^3. However, the most covalent $Fe_{III}N_{prox}$ bond in this series is found for myoglobin **MBR** (green circle with an H_ρ value of −0.0144 Hartree/Bohr^3), whereas as beet phytoglobin **PBE** (orange triangle) is found in the less covalent region. Both the distal and proximal ferrous FeN bonds are less covalent in character as reflected by average H_ρ values of −0.0038 and −0.0035 Hartree/Bohr^3, respectively, compared with their ferric counterparts with average H_ρ values of −0.0108 and −0.0111 Hartree/Bohr^3, respectively. The corresponding gas phase FeN bonds show a covalency in the middle range. In comparison, we found average H_ρ values of −0.0030 Hartree/Bohr^3 for the FeN proximal bonds in carboxy-myoglobin[59] and carboxy-neuroglobins,[60] and average H_ρ values in the range of −0.0065 Hartree/Bohr^3 for the carboxy FeC bond, showing that the adaption of small molecules leads to more covalent iron-ligand bonding.

3.3 | FeN bond length and bond strength

A popular measure of the strength of an AB bond is the associated bond length R(AB). Badger published in 1934 his famous rule which predicts an inverse power relationship between bond length and bond strength for diatomic molecules, utilizing the normal force constant as bond strength measure.[81] Kraka, Larsson, and Cremer[63] extended Badger's original rule to polyatomic systems based on local mode force constants. Recently, we could confirm Badger's rule for iron-ligand bonds in carboxymyglobins[59] and carboxyneuroglobins.[60]

Figure 4A–D shows how the local mode force constants k^a(FeN) correlate with the corresponding bond distances R(FeN) for the FeN bonds investigated in this work. We find for each of the four different

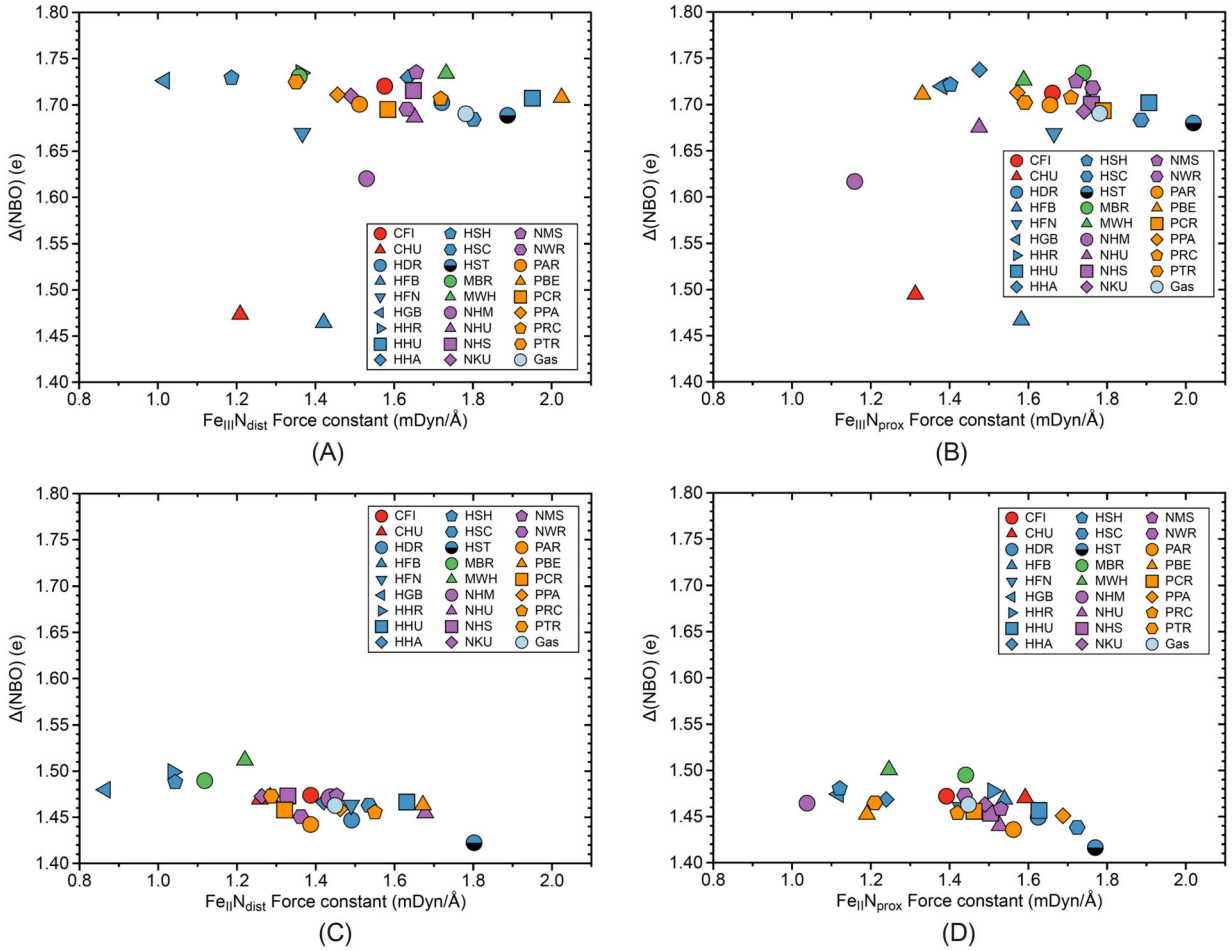

FIGURE 6 NBO atomic charge difference between Fe and N atoms as function of k^a(FeN); (A) $Fe_{III}N_{dist}$; (B) $Fe_{III}N_{prox}$; (C) $Fe_{II}N_{dist}$; and (D) $Fe_{II}N_{prox}$. In order to differentiate between the five groups cytoglobins are given in red, hemoglobins in blue, myoglobins in green, neuroglobins in purple and phytoglobins in orange color. The heme gas phase model is given in light–blue color. For protein labels see Table 1.

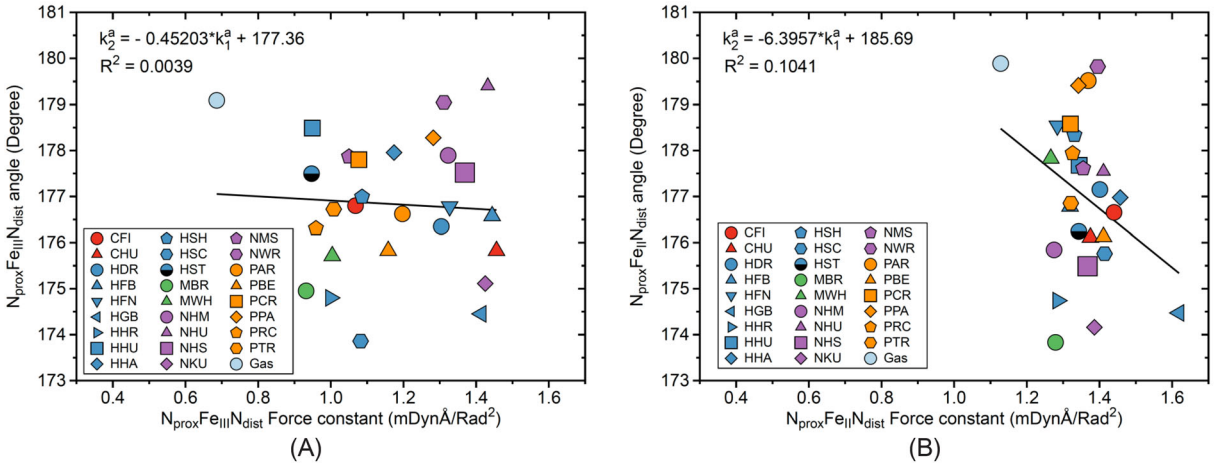

FIGURE 7 Correlation between k^a($N_{prox}FeN_{dist}$) and bond angle ($N_{prox}FeN_{dist}$); (A) Fe_{III} compounds; (B) Fe_{II} compounds. In order to differentiate between the five groups cytoglobins are given in red, hemoglobins in blue, myoglobins in green, neuroglobins in purple and phytoglobins in orange color. The heme gas phase model is given in light–blue color. For protein labels see Table 1.

FeN bond categories a trend, which shows that shorter FeN bonds are related to stronger FeN bonds, although there is no perfect inverse power relationship (see dashed lines in Figure 4A–D) as we found in our previous work on carboxymyglobins and carboxyneuroglobins. It can be explained by the fact that such a simple rule works best for a series of related compounds as seen in the protein systems

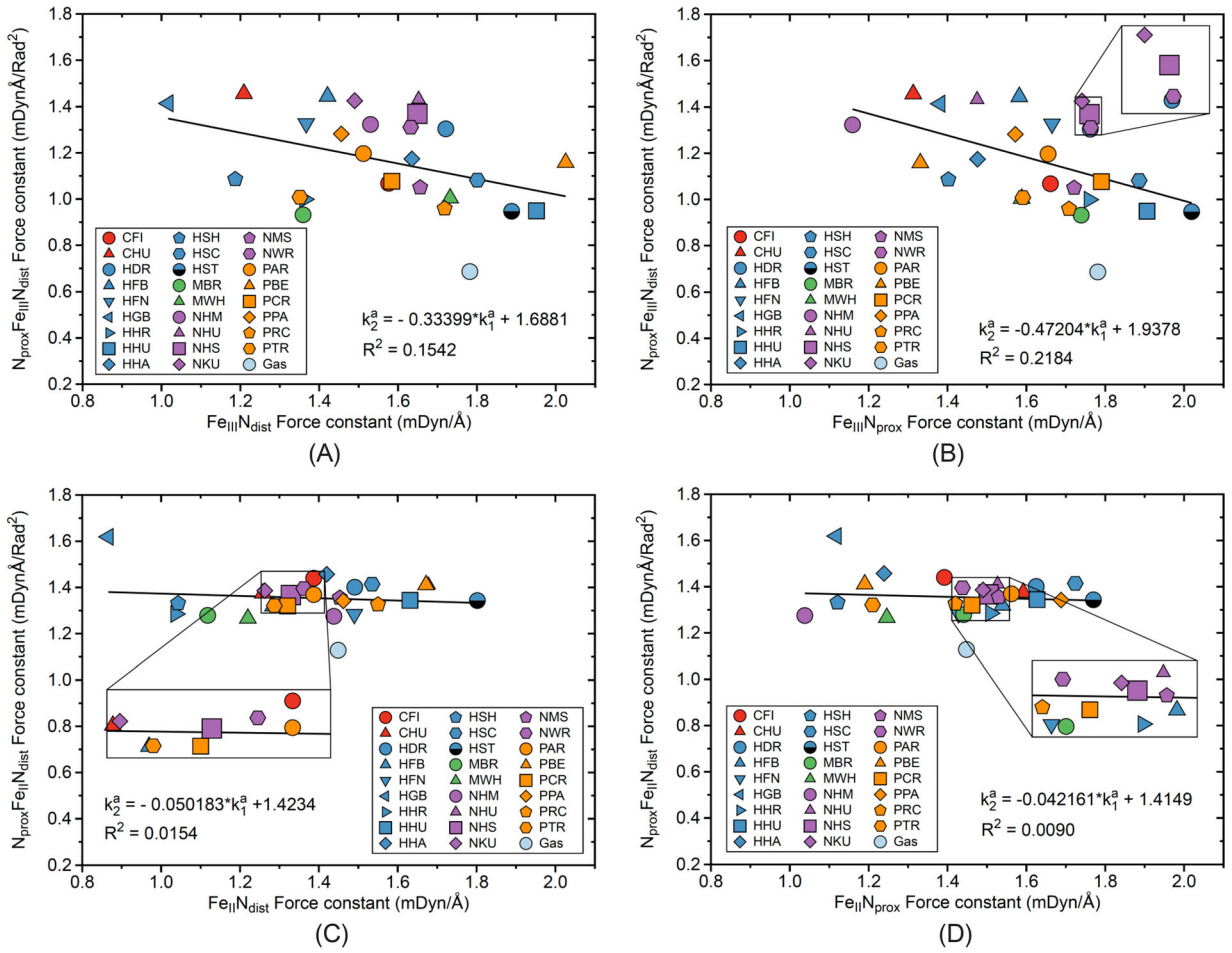

FIGURE 8 Correlation between $k^a(N_{prox}FeN_{dist})$ and $k^a(FeN)$; (A) $Fe_{III}N_{dist}$; (B) $Fe_{III}N_{prox}$; (C) $Fe_{II}N_{dist}$; and (D) $Fe_{II}N_{prox}$. In order to differentiate between the five groups cytoglobins are given in red, hemoglobins in blue, myoglobins in green, neuroglobins in purple and phytoglobins in orange color. The heme gas phase model is given in light–blue color. For protein labels see Table 1.

in the previous work,[25,26,82] rather than for a comparison of bonds in more diverse environments investigated in this study. Furthermore, the bond length is not always a qualified bond strength descriptor. Numerous cases have been reported illustrating that a shorter bond is not always a stronger bond.[83–85]

As depicted in Figure 4A, $Fe_{III}N_{dist}$ bond lengths stretch from 1.937 Å, beet phytoglobin **PBE** (orange triangle), to 2.039 Å, bacterium hemoglobin **HGB** (blue triangle). In comparison, $Fe_{III}N_{prox}$ bonds in Figure 4B, cover a smaller range which could be an indication that the heme pocket is tighter in this area. The shortest bond in this series with R(FeN) = 1.940 Å is that of bacterium hemoglobin **HST** (black–blue circle), and the longest with R(FeN) = 2.018 Å is that of beet phytoglobin **PBE** (orange triangle). It is interesting to note that **PBE** distal and proximal bond lengths are complementary, that is, the shorter distal bond corresponds to the longer proximal bond. The $Fe_{II}N_{dist}$ bond lengths shown in Figure 4C cover a range of 1.13 Å, which is somewhat larger than that of the ferric distal bond range, although this series covers a smaller range of local mode force constant values. The shortest bond in this series with R(FeN) = 1.945 Å is that of bacterium hemoglobin **HST** (black–blue circle), and the longest with R(FeN) = 2.058 Å is that of horse hemoglobin **HHR** (blue triangle). As for the ferric series, the proximal ferrous bonds in Figure 4D, cover a smaller range than their ferric counterparts. Shark hemoglobin **HSH** has the longest bond with R(FeN) = 2.027 Å in this series and bacterium hemoglobin **HST** has the shortest bond with R(FeN) = 1.951 Å. The gas phase FeN bond length of 1.650 Å (ferric) and 1.980 Å (ferrous) lies in both cases in the middle range.

With an overall average FeN bond length variation of only 0.12 Å (i.e., less than 6.5 % with regard to the smallest FeN bond), we conclude that the variation in the FeN bond properties is of electronic nature of the porphine ring, modified by the influence of the electrostatic potential of the protein active sites,[86] which is sensitively captured by the FeN local mode force constants.

3.4 | Comparison of local mode FeN force constants

To find out how the oxidation state effects the bond strength of the hemoproteins, Figure 5A–D present such a comparison between

the FeN distal and proximal bond strengths in the ferric and ferrous states. Although there is a relatively weak correlation, we observed that a larger FeN distal bond strength in the ferric state corresponds to an increase in the strength of this bond in the ferrous state as revealed by Figure 5A. In bacterium hemoglobin **HST** (black–blue circle), which is one of the strongest bonds investigated in this study in the ferric state (k^a = 1.888 mDyn/Å) and is also the strongest FeN distal bond in the ferrous state (k^a = 1.802 mDyn/Å). Similarly, the weakest FeN distal bond in the bacterium hemoglobin **HGB** (blue triangle) in the ferric state (k^a = 1.017 mDyn/Å), is also the weakest FeN distal bond in the ferrous state (k^a = 0.866 mDyn/Å). Figure 5B shows a correlation between the strength of the FeN proximal bonds in the ferric and the ferrous states, and although the correlation is much smaller than for the FeN distal bond strength reported above, it has a similar trend. The strongest FeN proximal bond in the bacterium hemoglobin **HST** (black–blue circle) in the ferric state (k^a = 2.019 mDyn/Å), is also the strongest proximal bond in the ferrous state (k^a = 1.770 mDyn/Å), and the weakest FeN proximal bond in the mutated human neuroglobin **NHM** (purple circle) in the ferric state (k^a = 1.159 mDyn/Å), is also the weakest in the ferrous state (k^a = 1.038 mDyn/Å). According to our analysis, we can generally conclude that the change of the protein oxidation state from ferric to the ferrous state of most of the investigated hemoproteins makes the FeN bond weaker, whether proximal or distal. However, the hemoproteins which have the strong FeN bond in the ferric state, also have a strong bond in the ferrous state, and the hemoproteins with the weak FeN bond in the ferric state, keep this bond weak in the ferrous state.

We can observe a broad trend indicating that the strength of the FeN distal bond is generally smaller than the strength of the FeN proximal bond in the ferric state in Figure 5C. We also observe a similar trend showing that the FeN distal bond is weaker than the proximal bond in the ferrous state in Figure 5D. Although there are studies showing that the FeN proximal bond in hemoproteins can be dissociated,[87–91] generally only the FeN distal bond is observed to be cleaved in the investigated hemoproteins, leaving the distal pocket to allow for endogenous small molecules to enter the distal pocket. Overall, our results show that there are a few hemoproteins that have the FeN distal bond stronger than the FeN proximal bond in both the ferric and the ferrous states, which could indicate an easier dissociation of the FeN proximal bond in these proteins rather than the distal bond. However, it is also commonly accepted that the dissociation of the FeN proximal bond is more difficult because there is a series of hydrogen bonds in the proximal heme pocket, which stabilizes the proximal histidine.[92–94] In this regard, our results encourage future experimental investigations digging deeper into this effect.

3.5 | FeN bond polarity and bond strength

Chemical bond theory[95,82,96] frequently discusses that a more polar AB bond often tends to be stronger than a related but less polar bond, using for example, bond dissociation energies (BDE)[97–99] as a bond strength measure. However, the BDE is a reaction parameter that includes all changes taking place during the dissociation process. Accordingly, it includes any (de)stabilization effects of the fragments to be formed after bond dissociation. It reflects the energy needed for bond breaking, but also contains energy contributions due to geometry relaxation and electron density reorganization in the dissociation fragments. Therefore, the BDE is not a suitable measure of the intrinsic strength of a chemical bond and its use may lead to a misjudgment of the intrinsic strength of a chemical bond.[62,100,101,102,103,104] We explored in this work the relationship between Fe and N NBO charge differences ΔNBO(FeN), serving as a measure of bond polarity, and k^a(FeN) serving as a measure of the intrinsic bond strength, for distal and proximal FeH bonds in both ferric and ferrous state. As revealed by Figure 6A–D there is no obvious trend that larger ΔNBO(FeN) values are related with larger k^a(FeN) values, as one may have assumed.

As shown in Figure 6A for most of $Fe_{III}N_{dist}$ bonds, the ΔNBO (FeN) values are in a range between 1.65 and 1.75 whereas k^a(FeN) values stretch from 1.0 to 2.0 mDyn/Å. There are two distinct outliers with considerably smaller ΔNBO(FeN) values than those found for the other protein systems in the ferric state, human cytoglobin **CHU** (red triangle), and fish hemoglobin **HFB** (blue triangle), with ΔNBO(FeN) of 1.473 and 1.464, respectively. Interesting to note is that the same pattern holds for the $Fe_{III}N_{prox}$ bonds as revealed by Figure 6B including the two outliers cytoglobin **CHU** (red triangle), and hemoglobin **HFB**(ΔNBO(FeN) of 1.495 and 1.467, respectively). As depicted in Figure 3A,B the small charge difference of those bonds is consistent with less negative H_ρ(FeN) values, indicating on the smallest covalent character of those bonds. Smaller covalency results in smaller electron density concentration in the middle of the bond, which becomes more equally distributed on the atoms, in turn leading to smaller ΔNBO (FeN) values. As is discussed in the next section, the **CHU** and **HFB** protein systems have relatively large NFeN bending force constants, indicating on a stiffer axial heme framework, all caused by the specific protein pocket of these two complexes. Also $Fe_{II}N_{dist}$ and $Fe_{II}N_{prox}$ bonds have a similar pattern, which is quite distinct from the Fe_{III}. Ferrous complexes have smaller bond polarization than their ferric counterparts, with ΔNBO(FeN) values ranging from 1.40 to 1.55. We also do not observe any outliers. The major difference between the ferric and ferrous compounds is related to the electronic structure of the heme group. In contrast to the closed shell ferrous electronic state, the ferric state is an open shell system with one unpaired electron leading to a smaller overall bond polarization. In conclusion, we can say that the individual protein environment sensitively polarizes the FeN bond, and a simple relationship between bond polarization and bond strength does not exist.

3.6 | NFeN axial bond angle

Whereas local stretching force constants k^a(AB) are the perfect tool for the assessment of the intrinsic strength of an AB bond, local

bending force constants k^a(ABC) provide a measure of bond angle stiffness, which we applied for example, to analyze and assess the Tolman cone angle[105] or to explore the bending of actinide sandwich complexes.[106] In this work, we used the local bond angle force constant $k^a(N_{dist}FeN_{prox})$ as a stiffness measure of the $N_{dist}FeN_{prox}$ axial bond of the heme group and investigated its relation to the distal and proximal local force constants $k^a(FeN_{dist})$ and $k^a(FeN_{prox})$, for both ferric and ferrous oxidation states. Results are illustrated in Figures 7A,B and 8A–D, and the corresponding data can be found in Table S5 of the Supplementary Material.

For the gas phase model **Gas**, we observe difference in the $N_{dist}FeN_{prox}$ axial bond angle between ferric and ferrous oxidation states (179.1 vs. 179.9 °), which in turn results in a considerable difference in the $k^a(N_{dist}FeN_{prox})$ values (0.686 vs. 1.128 mDynÅ/Rad^2). This indicates that the ferrous state, with an almost linear arrangement of the axial FeN bonds, has the Fe^{2+} radius bigger than Fe^{3+}, and is somewhat less flexible and more difficult to bent. However, for the protein systems, the situation is more complex, because the protein environment constrains the movement of the histidine side chains via space confinement (i.e., steric effect) and changes the electron density distribution in the heme part via electrostatic interactions between heme and the heme pocket. The $N_{dist}FeN_{prox}$ axial bond angle can only pick up the steric effect, however, the local mode bending force constant sensitively reflects the electronic effects caused by the protein electrostatic potential, which is not present in the gas phase, and is clearly shown in Figure 7A,B, disqualifying the bond angle as stiffness measure.

As depicted in Figure 8A,B all ferric $k^a(N_{dist}FeN_{prox})$ values are considerably larger than their gas phase counterpart, ranging from 0.932 mDynÅ/Rad^2, pig myoglobin **MBR** (green circle), to 1.456 mDynÅ/Rad^2, human cytoglobin **CHU** (red triangle), clearly reflecting the imposed space confinement of the protein pocket. We observe the overall trend as discussed for the gas phase molecular systems, namely that larger $k^a(N_{dist}FeN_{prox})$ are related to weaker FeN_{dist} bonds, see Figure 8A. The same holds also with regard to the FeN_{prox} bonds, as illustrated in Figure 8B. Figure 8C,D show the similar relation for the ferrous oxidation state. All ferrous $k^a(N_{dist}FeN_{prox})$ values are larger than the corresponding ferric ones, confirming what we found for the gas phase molecular system. It is interesting to note that compared to the ferric oxidation state, the gap between protein and gas phase bending force constants is smaller than that for the ferric state, reflecting that the axial ferrous part of the heme framework is less flexible, in line with the commonly accepted observation that the dissociation of the FeN proximal bond is more difficult because there is a series of hydrogen bonds in the proximal heme pocket, which stabilizes the proximal histidine.[92–94] In summary, the angle force constant $k^a(N_{dist}FeN_{prox})$ is a sensitive tool to monitor changes in the axial part of the heme framework, caused by the different protein environment, that is, reflecting that each protein structure has different amino acid geometries across different subgroups, which can change the confinement of the active site to allow for a more linear or less linear $N_{dist}FeN_{prox}$ angle, on top of the differences in the iron oxidation state.

3.7 | K-means analysis

In the absence of discernible clustering patterns among the five protein groups, we employed the K-means machine learning method[107,108] to gain insights into structurally related systems. Using data for the 26 proteins and their respective forms ($Fe_{II}N_{prox}$, $Fe_{II}N_{dist}$, $Fe_{III}N_{prox}$, and $Fe_{III}N_{dist}$), as well as a gas phase structure, we conducted K-means clustering analysis. The optimal number of clusters was determined using the elbow method (sum of squares error) and silhouette analysis. This analysis revealed the similarities and differences in each cluster group as we transitioned from ferrous to ferric and from proximal to distal FeN bond. The data used for the machine-

TABLE 2 K-means clustering groups for hemoproteins and gas phase model, investigated in this study.

Cluster	$Fe_{II}N_{prox}$	$Fe_{III}N_{prox}$	$Fe_{II}N_{dist}$	$Fe_{III}N_{dist}$
Cluster 1	**HGB**	**CHU**	**HGB**	**CHU**
	HSH	**NHM**	**HHR**	**HGB**
	NHM		**HSH**	**HSH**
Cluster 2	**HHA**	**HGB**		**HFN**
	MWH	**HHA**		**HHR**
	PBE	**HSH**	**MBR**	**MBR**
	PTR	**NHU**		**PPA**
		PBE		**PTR**
Cluster 3	**CFI**	**CFI**	**CHU**	**HFB**
	HFN	**HFB**	**HFB**	**NHM**
	MBR	**HFN**	**MWH**	**NKU**
	NWR	**MWH**	**NHS**	**PAR**
	PCR	**PAR**	**NWR**	
	PRC	**PPA**	**NKU**	
	Gas	**PTR**	**PCR**	
			PTR	
Cluster 4	**CHU**	**HDR**	**CFI**	**CFI**
	HFB	**HHR**	**HDR**	**HDR**
	HHR	**MBR**	**HFN**	**HHA**
	NHU	**NHS**	**HHA**	**MWH**
	NHS	**NKU**	**HSC**	**NHU**
	NKU	**NMS**	**NHM**	**NHS**
	NMS	**NWR**	**NMS**	**NMS**
	PAR	**PCR**	**PAR**	**NWR**
		PRC	**PPA**	**PCR**
		Gas	**PRC**	**PRC**
			Gas	
Cluster 5	**HDR**	**HHU**	**HHU**	**HHU**
	HHU	**HSC**	**HST**	**HSC**
	HSC	**HST**	**NHU**	**HST**
	HST		**PBE**	**PBE**
	PPA			**Gas**

learning method included the distance between Fe and N, local force constant, energy density, and charge difference from NBO. The resulting cluster groups for the 26 proteins and gas phase structure are presented in Table 2. Figures S1–S4 of Supplementary Material show the results of clustering in different colors of the BSO, the bond length, the energy density and the charge difference, as a function of the local mode force constant k^a.

Notably, as we transitioned from ferrous to ferric for the FeN proximal bond, significant shifts in cluster grouping were observed for **CHU**, **PPA**, and **NHU**, highlighting the evident influence of the transition. Conversely, the remaining proteins remained relatively consistent in their respective cluster groups. Similar trends were noticed when transitioning from ferrous to ferric for the FeN distal bond, particularly with **CHU** and **PPA**, indicating the significant impact of the iron charge on these two protein groups. Additionally, transitioning from proximal to distal, irrespective of the charge of Fe, resulted in discernible differences for **NHM**, **HHA**, and **PBE**. In summary, the K-Means analysis perfectly rounds off our findings that the protein environment is primarily influenced by the proximal and distal positioning, rather than the charge of the Fe atom.

4 | CONCLUSIONS

In this study, we analyzed the strength of the distal and proximal FeN bonds and explore if these FeN bond strengths show a correlation between each group in a series of bishistidyl hemoproteins, as well as to describe the stiffness of the axial NFeN bond angle, in both the ferric and ferrous oxidation states. Utilizing LMA, NBO, and QTAIM based on QM/MM calculations starting from available x-ray experimental structures, we investigated hemoproteins from bacteria, animals, human, and plants, which involved two cytoglobins, ten hemoglobins, two myoglobins, six neuroglobins, and six phytoglobins. Our results highlight that protein effects are sensitively measured and reflected in local mode force constants, allowing one to investigate trends in diverse protein groups. We also concluded that the strength of the distal FeN bond is not the key parameter for distal histidine dissociation, nor the primary cause of diverse biological activities of the investigated hemoproteins, as one might have assumed. This is reflected by the fact that the bond strengths do not cluster according to the protein groups from different species. We have found that there is only a moderate correlation between the strength of both the distal and proximal FeN bonds and the bond length as well as the energy density taken at a bond critical point, qualifying the local mode force constant as a sensitive measure of bond strength capturing both steric and electronic effects. We have observed that the FeN bond length does not vary much, indicating the FeN bond properties are of electronic nature, and can conclude that the change of the protein oxidation state from ferric to ferrous state generally makes the FeN bond weaker, whether proximal or distal. This is also reflected by the somewhat reduced covalency of the ferrous complexes. We also show that there is no simple relationship between bond polarization and bond strength and that the individual protein environment is able to sensitively polarize the FeN bond. Another interesting result of our investigation is that the NFeN bond angles do not reflect electronic effects caused by the protein electrostatic potential, and therefore disqualify using the bond angle as a stiffness measure. Instead, the bending local force constant is sensitive enough to monitor changes that are caused by different protein environments, as well as differences in the Fe oxidation states. Overall, our comprehensive computational study shows the impact of utilizing a variety of quantitative molecular bond properties, such as local vibrational mode force constants k^a(FeN) and k^a(NFeN), that could serve as a guideline for future experimental studies of bishistidyl hemoproteins and that provide to a more holistic view by complementing macroscopic properties such as rate constants with important details at the molecular level.

ACKNOWLEDGMENTS

This work was financially supported by the National Science Foundation (Grants CHE 2102461 and DGE 2034834). The authors thank SMU's Center for Scientific Computing for providing generous computational resources.

DATA AVAILABILITY STATEMENT

The data that support the findings of this study are available from the corresponding author upon reasonable request.

ORCID

Marek Freindorf https://orcid.org/0000-0001-5285-5455

REFERENCES

[1] C. J. Reedy, B. R. Gibney, *Chem. Rev.* **2004**, *104*, 617.
[2] Y.-W. Lin, J. Wang, *J. Inorg. Biochem.* **2013**, *129*, 162.
[3] X. Huang, J. T. Groves, *Chem. Rev.* **2018**, *118*, 2491.
[4] H. Kitagishi, Q. Mao, *Polym. J.* **2022**, *2022*, 465.
[5] Y. Yuan, M. F. Tam, V. Simplaceanu, C. Ho, *Chem. Rev.* **2015**, *115*, 1702.
[6] H. B. Gray, J. R. Winkler, *Annu. Rev. Biochem.* **1996**, *65*, 537.
[7] T. L. Poulos, *Chem. Rev.* **2014**, *114*, 3919.
[8] H. Sawai, N. Kawada, K. Yoshizato, H. Nakajima, S. Aono, Y. Shiro, *Biochemistry* **2003**, *42*, 5133.
[9] J. T. Trent, S. Kundu, J. A. Hoy, M. S. Hargrove, *J. Mol. Biol.* **2004**, *341*, 1097.
[10] D. de Sanctis, A. Pesce, M. Nardini, M. Bolognesi, A. Bocedi, P. Ascenzi, *IUBMB Life* **2004**, *56*, 643.
[11] D. de Sanctis, S. Dewilde, C. Vonrhein, A. Pesce, L. Moens, P. Ascenzi, T. Hankeln, T. Burmester, M. Ponassi, M. Nardini, et al., *J. Biol. Chem.* **2005**, *280*, 27222.
[12] A. Pesce, K. Barmpidi, S. Dewilde, C. Estarellas, L. Moens, M. Bolognesi, F. J. Luque, M. Nardini, *J. Inorg. Biochem.* **2023**, *246*, 112289.
[13] J. T. Trent, A. N. Hvitved, M. S. Hargrove, *Biochemistry* **2001**, *40*, 6155.
[14] J. Uzan, S. Dewilde, T. Burmester, T. Hankeln, L. Moens, D. Hamdane, M. C. Marden, L. Kiger, *Biophys. J.* **2004**, *87*, 1196.
[15] T. R. Weiland, S. Kundu, J. T. Trent, J. A. Hoy, M. S. Hargrove, *J. Am. Chem. Soc.* **2004**, *126*, 11930.
[16] B. J. Smagghe, G. Sarath, E. Ross, J. Hilbert, M. S. Hargrove, *Biochemistry* **2006**, *45*, 561.
[17] B. J. Smagghe, P. Halder, M. S. Hargrove, R. K. Poole, *Chapter Twenty – Measurement of Distal Histidine Coordination Equilibrium and Kinetics in Hexacoordinate Hemoglobins*, Vol. 436, Academic Press, Amsterdam, Netherlands **2008**, p. 359.

[18] S. Kakar, F. G. Hoffman, J. F. Storz, M. Fabian, M. S. Hargrove, *Biophys. Chem.* **2010**, *152*, 1.
[19] A. Bocahut, V. Derrien, S. Bernad, P. Sebban, S. Sacquin-Mora, E. Guittet, E. Lescop, *J. Biol. Inorg. Chem.* **2013**, *18*, 111.
[20] G. DeSimone, D. Sbardella, F. Oddone, A. Pesce, M. Coletta, P. Ascenzi, *Cell* **2023**, *10*, 3366.
[21] P. Halder, J. T. Trent III, M. S. Hargrove, *Proteins* **2007**, *66*, 172.
[22] P. P. Samuel, D. A. Case, *Biochemistry* **2020**, *59*, 4093.
[23] A. Merlino, A. Vergara, F. Sica, L. Mazzarella, *Marine Genom.* **2009**, *2*, 51.
[24] D. M. A. Smith, M. Dupuis, E. R. Vorpagel, T. P. Straatsma, *J. Am. Chem. Soc.* **2003**, *125*, 2711.
[25] E. Kraka, W. Zou, Y. Tao, *WIREs: Comput. Mol. Sci.* **2020**, *10*, 1480.
[26] E. Kraka, M. Quintano, H. W. L. Force, J. J. Antonio, M. Freindorf, *J. Phys. Chem. A* **2022**, *126*, 8781.
[27] R. F. W. Bader, *Monatsh. Chem.* **2005**, *136*, 819.
[28] A. E. Reed, L. A. Curtiss, F. Weinhold, *Chem. Rev.* **1988**, *88*, 899.
[29] D. Giordano, A. Pesce, S. Vermeylen, S. Abbruzzetti, M. Nardini, F. Marchesani, H. Berghmans, C. Seira, S. Bruno, F. Javier Luque, et al., *Comput. Struct. Biotechnol. J.* **2020**, *18*, 2132.
[30] M. Makino, H. Sugimoto, H. Sawai, N. Kawada, K. Yoshizato, Y. Shiro, *Acta Crystall. D* **2006**, *62*, 671.
[31] L. Vitagliano, G. Bonomi, A. Riccio, G. di Prisco, G. Smulevich, L. Mazzarella, *Europ. J. Biochem.* **2004**, *271*, 1651.
[32] A. Riccio, L. Vitagliano, G. di Prisco, A. Zagari, L. Mazzarella, *Proc. Natl. Acad. Sci. U. S. A.* **2002**, *99*, 9801.
[33] A. Pesce, L. Thijs, M. Nardini, F. Desmet, L. Sisinni, L. Gourlay, A. Bolli, M. Coletta, S. Van Doorslaer, X. Wan, et al., *J. Mol. Biol.* **2009**, *386*, 246.
[34] V. L. Robinson, B. B. Smith, A. Arnone, *Biochemistry* **2003**, *42*, 10113.
[35] J. Yi, Human (Alpha Met/Beta Hemichrome) Hemoglobin with s–Nitrosation at beta–cys93, the Protein Data Bank ID: 6NQ5. **2020** https://doi.org/10.2210/pdb6NQ5/pdb
[36] L. Feng, S. Zhou, L. Gu, D. A. Gell, J. P. Mackay, M. J. Weiss, A. J. Gow, Y. Shi, *Nature* **2005**, *435*, 697.
[37] P. Ramesh, S. S. Sundaresan, P. Sathya Moorthy, M. Balasubramanian, M. N. Ponnuswamy, *J. Synch. Rad.* **2013**, *20*, 843.
[38] B. B. Wenke, J. T. J. Lecomte, A. Héroux, J. L. Schlessman, *Proteins* **2014**, *82*, 528.
[39] J. A. Hoy, S. Kundu, J. T. Trent, S. Ramaswamy, M. S. Hargrove, *J. Biol. Chem.* **2004**, *279*, 16535.
[40] Y. Dou, S. J. Admiraal, M. Ikeda-Saito, S. Krzywda, A. J. Wilkinson, T. Li, J. S. Olson, R. C. Prince, I. J. Pickering, G. N. George, *J. Biol. Chem.* **1995**, *270*, 15993.
[41] J.-F. Du, W. Li, L. Li, G.-B. Wen, Y.-W. Lin, X. Tan, *ChemistryOpen* **2015**, *4*, 97.
[42] S.-Q. Gao, H. Yuan, X.-C. Liu, L. Li, X. Tan, G.-B. Wen, Y.-W. Lin, *Proteins* **2022**, *90*, 1152.
[43] A. Pesce, S. Dewilde, M. Nardini, L. Moens, P. Ascenzi, T. Hankeln, T. Burmester, M. Bolognesi, *Structure* **2003**, *11*, 1087.
[44] B. G. Guimarães, D. Hamdane, C. Lechauve, M. C. Marden, B. Golinelli-Pimpaneau, *Acta Crystall. D* **2014**, *70*, 1005.
[45] J. Kim, Y. Fukuda, T. Inoue, *Febs J.* **2019**, *286*, 1287.
[46] B. Vallone, K. Nienhaus, M. Brunori, G. U. Nienhaus, *Proteins* **2004**, *56*, 85.
[47] S. De Henau, L. Tilleman, M. Vangheel, E. Luyckx, S. Trashin, M. Pauwels, F. Germani, C. Vlaeminck, J. R. Vanfleteren, W. Bert, et al., *Nature Comm.* **2015**, *6*, 8782.
[48] N. Mukhi, S. Dhindwal, S. Uppal, P. Kumar, J. Kaur, S. Kundu, *Biochim. Biophys. Acta* **2013**, *1834*, 1944.
[49] S. Christensen, L. Groth, N. Leiva-Eriksson, M. Nyblom, L. Bülow, *Antioxidants* **2022**, *11*, 1615.
[50] B. Smagghe, J. Hoy, M. Hargrove, The crystal structure of nonsymbiotic corn hemoglobin 1, The Protein Data Bank ID: 2R50. **2007** https://doi.org/10.2210/pdb2R50/pdb
[51] S. Kakar, R. Sturms, A. Tiffany, J. C. Nix, A. A. DiSpirito, M. S. Hargrove, *Biochemistry* **2011**, *50*, 4273.
[52] M. S. Hargrove, E. A. Brucker, B. Stec, G. Sarath, R. Arredondo-Peter, R. V. Klucas, J. S. Olson, G. N. Phillips, *Structure* **2000**, *8*, 1005.
[53] J. D. Kelley, J. J. Leventhal, *Problems in Classical and Quantum Mechanics: Normal Modes and Coordinates*, Springer, London, England **2017**.
[54] S. Califano, *Vibrational States*, Wiley, London **1976**.
[55] E. B. Wilson, J. C. Decius, P. C. M. Cross, *Molecular Vibrations, The Theory of Infrared and Raman Vibrational Spectra*, McGraw-Hill, New York **1955**.
[56] E. B. Wilson, *J. Chem. Phys.* **1941**, *9*, 76.
[57] Z. Konkoli, D. Cremer, *Int. J. Quantum Chem.* **1998**, *67*, 1.
[58] Z. Konkoli, J. A. Larsson, D. Cremer, *Int. J. Quantum Chem.* **1998**, *67*, 11.
[59] M. Freindorf, E. Kraka, *J. Mol. Model.* **2020**, *26*, 281.
[60] M. Freindorf, A. A. A. Delgado, E. Kraka, *J. Comput. Chem.* **2022**, *43*, 1725.
[61] J. J. Antonio, E. Kraka, *Biochemistry* **2023**, *62*, 2325.
[62] D. Cremer, E. Kraka, *Curr. Org. Chem.* **2010**, *14*, 1524.
[63] E. Kraka, J. A. Larsson, D. Cremer, in *Computational Spectroscopy* (Ed: J. Grunenberg), Wiley, New York **2010**, p. 105.
[64] I. Mayer, *Chem. Phys. Lett.* **1983**, *97*, 270.
[65] I. Mayer, *Int. J. Quantum Chem.* **1986**, *29*, 477.
[66] I. Mayer, *J. Comput. Chem.* **2007**, *28*, 204.
[67] C. Adamo, V. Barone, *J. Chem. Phys.* **1999**, *110*, 6158.
[68] R. Ditchfield, W. J. Hehre, J. A. Pople, *J. Chem. Phys.* **1971**, *54*, 724.
[69] L. W. Chung, W. M. C. Sameera, R. Ramozzi, A. J. Page, M. Hatanaka, G. P. Petrova, T. V. Harris, X. Li, Z. Ke, F. Liu, et al., *Chem. Rev.* **2015**, *115*, 5678.
[70] D. A. Case, I. Y. Ben-Shalom, S. R. Brozell, D. S. Cerutti, T. E. Cheatham, V. W. D. Cruzeiro, T. A. Darden, R. E. Duke, D. Ghoreishi, M. K. Gilson, et al., *Amber*, University of California, San Francisco **2018**.
[71] W. L. Jorgensen, J. Chandrasekhar, J. D. Madura, R. W. Impey, M. L. Klein, *J. Chem. Phys.* **1983**, *79*, 926.
[72] S. Zhao, Z.-H. Li, W.-N. Wang, Z.-P. Liu, K.-N. Fan, Y. Xie, H. F. Schaefer, *J. Chem. Phys.* **2006**, *124*, 184102.
[73] C. J. Cramer, D. G. Truhlar, *Phys. Chem. Chem. Phys.* **2009**, *11*, 10757.
[74] S. Li, J. M. Hennigan, D. A. Dixon, K. A. Peterson, *J.Phys. Chem. A* **2009**, *113*, 7861.
[75] M. K. Safo, G. P. Gupta, F. A. Walker, W. R. Scheidt, *J. Am. Chem. Soc.* **1991**, *113*, 5497.
[76] J. Wang, A. D. Becke, J. Vedene, H. Smith, *J. Chem. Phys.* **1995**, *102*, 3477.
[77] M. J. Frisch, G. W. Trucks, H. B. Schlegel, G. E. Scuseria, M. A. Robb, J. R. Cheeseman, G. Scalmani, V. Barone, G. A. Petersson, H. Nakatsuji, et al., *Gaussian 16*, Gaussian Inc, Wallingford CT **2016**.
[78] W. Zou, R. Moura Jr., M. Quintano, F. Bodo, Y. Tao, M. Freindorf, M. Z. Makoś, N. Verma, D. Cremer, E. Kraka, LModeA2023, *Computational and Theoretical Chemistry Group (CATCO)*, Southern Methodist University, Dallas, TX, USA **2023**.
[79] T. A. Keith, *Aimall*, TK Gristmill Software, Overland Park KS **2017**.
[80] E. D. Glendening, J. K. Badenhoop, A. E. Reed, J. E. Carpenter, J. A. Bohmann, C. M. Morales, C. R. Landis, F. Weinhold, *Nbo6*, Theoretical Chemistry Institute, University of Wisconsin, Madison **2013**.
[81] R. M. Badger, *J. Chem. Phys.* **1934**, *2*, 128.
[82] L. Zhao, M. Zhi, G. Frenking, *Chem. – Eur. J.* **2021**, *27*, e26773.
[83] E. Kraka, D. Cremer, *Rev. Proc. Quim.* **2012**, *2012*, 39.
[84] E. Kraka, D. Setiawan, D. Cremer, *J. Comput. Chem.* **2015**, *37*, 130.
[85] M. Kaupp, D. Danovich, S. Shaik, *Coord. Chem. Rev.* **2017**, *344*, 355.
[86] Z. Ji, J. Kozuch, I. I. Mathews, C. S. Diercks, Y. Shamsudin, M. A. Schulz, S. G. Boxer, *J. Am. Chem. Soc.* **2022**, *144*, 20947.
[87] P. Ascenzi, M. Coletta, A. Desideri, M. Brunori, *Biochim. Biophys. Acta* **1985**, *829*, 299.

[88] Q. Tang, W. A. Kalsbeck, J. S. Olson, D. F. Bocian, *Biochemistry* **1998**, *37*, 7047.
[89] Z. Dai, E. R. Farquhar, D. P. Arora, E. M. Boon, *Dalton Trans.* **2012**, *41*, 7984.
[90] S. Muralidharan, E. M. Boon, *J. Am. Chem. Soc.* **2012**, *134*, 2044.
[91] M. A. Herzik, R. Jonnalagadda, J. Kuriyan, M. A. Marletta, *Proc. Natl. Acad. Sci. U. S. A.* **2014**, *111*, E4156.
[92] R. G. Douglas, D. L. Rousseau, *J. Struct. Biol.* **1992**, *109*, 13.
[93] E. C. Liong, Y. Dou, E. E. Scott, J. S. Olson, G. N. Phillips, *J. Biol. Chem.* **2001**, *276*, 9093.
[94] S. Kundu, B. Snyder, K. Das, P. Chowdhury, J. Park, J. W. Petrich, M. S. Hargrove, *Proteins* **2002**, *46*, 268.
[95] L. Pauling, *The Nature of the Chemical Bond*, Cornell University Press, New York **1960**.
[96] E. Blokker, X. Sun, J. Poater, T. A. H. J. Martijn van der Schuur, F. M. Bickelhaupt, *Int. J. Quantum Chem.* **2021**, *122*, 15616.
[97] Y.-R. Luo, *Comprehensive Handbook of Chemical Bond Energies*, Taylor and Francis, Boca Raton, FL **2007**.
[98] M. D. Morse, *Acc. Chem. Res.* **2018**, *52*, 119.
[99] L. Zhao, M. Hermann, W. H. E. Schwarz, G. Frenking, *Nat. Rev. Chem.* **2019**, *3*, 49.
[100] R. Kalescky, E. Kraka, D. Cremer, *Int. J. Quantum Chem.* **2014**, *114*, 1060.
[101] R. Kalescky, W. Zou, E. Kraka, D. Cremer, *J. Phys. Chem. A* **2014**, *118*, 1948.
[102] V. Oliveira, E. Kraka, D. Cremer, *Inorg. Chem.* **2016**, *56*, 488.
[103] D. Setiawan, D. Sethio, D. Cremer, E. Kraka, *Phys. Chem. Chem. Phys.* **2018**, *20*, 23913.
[104] D. Sethio, V. Oliveira, E. Kraka, *Molecules* **2018**, *23*, 2763.
[105] D. Cremer, *WIREs Comput. Mol. Sci.* **2013**, *3*, 482.
[106] M. Z. Makoś, W. Zou, M. Freindorf, E. Kraka, *Mol. Phys.* **2020**, *2020*, e1768314.
[107] S. Lloyd, *IEEE Trans. Inf. Theory* **1982**, *28*, 129.
[108] J. MacQueen, *Proceedings of the fifth Berkeley symposium on mathematical statistics and probability*, Vol. 1, University of California Press, Oakland, CA, USA **1967**, p. 281.

SUPPORTING INFORMATION

Additional supporting information can be found online in the Supporting Information section at the end of this article.

How to cite this article: M. Freindorf, J. J. Antonio, E. Kraka, *J. Comput. Chem.* **2023**, 1. https://doi.org/10.1002/jcc.27267